A Flexible Metal-Organic Framework: Guest Molecules Controlled Dynamic Gas Adsorption

Yanfeng Yue,[†, ξ] Jeremy A. Rabone,[‡] Hongjun Liu,[†] Shannon M. Mahurin,[,†] Man-Rong Li,[δ] Hailong Wang,[ξ] Zhengliang Lu,[ϕ] Banglin Chen,[*, ξ] Jihang Wang,[⊥] Youxing Fang,[†] and Sheng Dai[*,†,η]*

[†]Chemical Sciences Division, Oak Ridge National Laboratory, Oak Ridge, Tennessee 37831, USA

[‡]Castet-naü, Quartier Gey, Sarrance 64490, France

[δ]Department of Chemistry and Chemical Biology, Rutgers, The State University of New Jersey, Piscataway, New Jersey 08854, USA

[ξ]Department of Chemistry, University of Texas at San Antonio, One UTSA Circle, San Antonio, Texas 78249, USA

[ϕ]School of Chemistry and Chemical Engineering, University of Jinan, Jinan 250022, P. R. China

[⊥]Department of Chemistry, Cornell College, Mount Vernon, Iowa 52314, USA

[η]Department of Chemistry, University of Tennessee, Knoxville, Tennessee 37996, USA

ABSTRACT A flexible metal-organic framework (MOF) of $[Zn_3(btca)_2(OH)_2]\cdot(guest)_n$ (H_2btca = 1,2,3-benzotriazole-5-carboxylic acid) that exhibits guest molecule-controlled dynamic gas adsorption is reported in which carbon dioxide molecules rather than N_2, He, and Ar induce a structural transition with a corresponding appearance of additional steps in the isotherms. Physical insights into the dynamic adsorption behaviors of flexible compound **1** were detected by gas adsorption at different temperatures and different pressures and confirmed by Fourier transform infrared spectroscopy and molecular simulations. Interestingly, by taking advantage of the flexible nature inherent to the framework, this MOF material enables highly selective adsorption of CO_2/N_2, CO_2/Ar, and CO_2/He, of 36.3, 32.6, and 35.9, respectively at 298 K. This class of flexible MOFs has potential applications for controlled release, molecular sensing, noble gas separation, smart membranes, as well as nanotechnological devices.

Keywords: Dynamic adsorption • Monte Carlo simulation • Selective adsorption • Variable pressure FT-IR

INTRODUCTION

Metal-organic frameworks (MOFs), which are typically porous, are a modern development on the interface between coordination chemistry and material science. These materials show hybrid functionality that integrates inorganic building units (SBUs) (formed in situ) and multidentate organic ligands.[1–25] The periodic and porous structures give them advantages for applications such as gas storage, gas purification, catalysis, sensing and large molecule adsorption where precise control of the structure leads to specific behaviors.[26–30] However, in contrast to the rigid framework of inorganic porous solids such as zeolites, the most remarkable feature of many MOFs is their structural flexibility.[31–36] Structural transformations upon the adsorption and

desorption of guest molecules, also known as guest-induced switching, can radically alter the characteristics of such flexible MOFs. For guest-induced structural switching that generates large changes in pore volume, the terms “breathing” and “breathing effect” are applied. MOFs that exhibit the breathing effect are one of the most promising developments of MOF chemistry that have potential for selective sorption.[37–41]

The preparation of breathing MOFs is usually associated with a flexible coordination environment (i.e. where the coordination between metal and ligands can reversibly reconfigure) and the dynamic effect is typically associated with a large change of the internal pore volume.[42] Such flexible porous MOF solids typically exhibit a precise “gate-opening” pressure identifiable from steps in the isotherm, where the free-energy cost of the structural rearrangements necessary to open the structure is compensated by the free energy associated with the sorption of guest molecules. Besides the appearance of steps in the adsorption isotherm, appreciable hysteresis is often observed for these materials owing to host-guest interactions.[43]

Although the number of MOFs has grown exponentially since the 1970’s, the understanding of the breathing behaviors many MOFs exhibit still represents a formidable challenge. Investigations are hampered by the need for rather large specimens that exhibit a prominent guest-induced structural transformation to allow a high degree of certainty in determining the structural transformations at play. The archetypical representatives of the breathing MOFs are the MIL-53 type structures. The MIL-53 structures $M^{III}(OH)\cdot BDC$ (M=Al, Cr, Fe, Ga; BDC = 1,4-benzenedicarboxylate),[42,44,45] are built up from chains of metal-centered octahedra with corner sharing OH vertices that are further interlinked into three-dimensional trellis-like structures by rigid 1,4-benzenedicarboxylate ligands, resulting in one-dimensional channels. Upon thermally activated sorption and desorption, the MIL-53 structure can open and close like

a trellis with a high degree of expansion and contraction of the pores.[42] Although a great deal is known about the dynamic adsorption in flexible MOF materials, the understanding of the more subtle effects of breathing behavior in MOFs beyond simple gate-opening stimuli such as guest molecules is very limited.[46] Herein, we present an investigation into the dynamics of the different guest gas adsorption behaviors of a flexible zinc compound $[Zn_3(btca)_2(OH)_2]\cdot(DMF)$ (H_2btca = 1,2,3-benzotriazole-5-carboxylic acid; DMF = N,N-dimethylformamide), **1**. Carbon dioxide molecules controlled dynamic adsorption was observed where MOF breathing was dependent on the specific interaction between the intrinsic properties of guests and the framework as confirmed by variable pressure Fourier transform infrared (FT-IR) spectroscopy and investigated by quantitative computational modeling. It is especially noteworthy that the flexible nature inherent to the framework enables the highly selective adsorption of CO_2/N_2, CO_2/Ar, and CO_2/He with selectivies of 36.3, 32.6, and 35.9, respectively, at room temperature.

EXPERIMENTAL DETAILS

Synthesis. Zinc(II) acetate dihydrate (0.022g, 0.1 mmol) and H_2btca (0.016g, 0.1 mmol) were added to an autoclave containing 1.0 mL water, 0.5 mL DMF and 2.0 mL 0.1 M NaOH aqueous solution and the mixture was sonicated for 10 min. Then the autoclave was closed tightly and heated to 150 ^{o}C and kept at that temperature for 4 days. The resulting brown crystals were washed with ethanol and dried under vacuum at 60 ^{o}C overnight before characterization, including variable pressure Fourier transform infrared (FT-IR), powder x-ray diffraction (XRD), nitrogen adsorption-desorption measurements at 77K, CO_2, N_2, Ar, and He adsorption-desorption, high pressure CO_2 and N_2 adsorption-desorption and elemental analysis.

Characterization. Thermogravimetric analysis (TGA) was carried out using a TA Instrument 2950 from room temperature to 900 ^{o}C at a heating rate of 5 ^{o}C min^{-1} under air atmosphere. The

elemental analysis was conducted at Galbraith Laboratories Inc.. Powder XRD patterns were recorded on a Bruker D8-Advance diffractometer (in Bragg-Brentano geometry (λ = 1.5406 Å): Cu *K*α radiation, SOL-X solid state detector, 40 kV and 40 mA, step scan 5–60º/0.02º/15 s. The sample was covered with oil to isolate from air during the data collection. The Le Bail phase fitting was performed with the EXPGUI interface of GSAS programs.[47]

X-ray single crystal structure data of compound **1** were collected with a Rigaku Saturn 724 diffractometer with graphite-monochromated Mo-*K*α (λ = 0.71073 Å) radiation at 293 K. Empirical absorption corrections were applied to the data using the SADABS program.[48] The structure was solved by the direct method and refined by the full-matrix least squares on *F*2 using the SHELXS-86 and SHELXL-97 programs.[49] All non-hydrogen atoms were refined anisotropically. All hydrogen atoms attached to carbon atoms were placed at their ideal positions. Crystallographic data and structure determination summaries are given in Table S1.

Crystallographic data (excluding structure factors) for the structures in this paper have been deposited with the Cambridge Crystallographic Data Centre, CCDC, 12 Union Road, Cambridge CB21EZ, UK. Copies of the data can be obtained free of charge on quoting the depository numbers CCDC-1045659 for compound **1** (Fax: +44-1223-336-033; E-Mail: deposit@ccdc.cam.ac.uk, http://www.ccdc.cam.ac.uk).

N_2 adsorption studies were performed to confirm the permanent porosity of compound 1, as well as to determine the surface area. Gas adsorption experiments were performed on a Micromeritics Tristar 3000 at 77 K. Before gas permeation tests, the as-synthesized compound 1 was activated at 150 °C under Ar flow for more than 12 hours to remove the occluded guest molecules in the channels, and subsequently loaded for adsorption analysis. CO_2, N_2, Ar, and He isotherms and high pressure isotherms of CO_2 and N_2 were carried out using an IGA-002

Intelligent Gravimetric Analyser supplied by Hiden Analytical Ltd. A 30 mg sample was loaded into the sample boat and heated to 150 °C under vacuum (~ 10^{-5} bar) for 12 hours. The sample was then cooled to 25 °C under vacuum and the dry mass was recorded. For all isotherms, the temperature of the sample was maintained within ±0.1 °C of the desired temperature and the sample chamber was pressurized to a set pressure of the adsorbate and allowed to equilibrate for a minimum of 40 min before moving to the next pressure point.

Modeling. Molecular dynamics simulations were carried out using the GAFF force field supplemented by a set of angular terms to maintain metal coordinated structure. A supercell of 6 × 6 × 6 loaded with the equivalent of 12 molecules of CO_2 per unit cell was constructed from solvated unit cell structure. A series of NσT (constant number, stress and temperature) ensemble molecular dynamics simulations were carried out to simulate the desorption process. After collection of statistics for each simulation, several CO_2 molecules were randomly removed from the simulation cell, followed by re-equilibration of 10 ps and further production simulation of 10 ps. The sorption module of Material Studio was used to perform isotherm simulations. The COMPASS force field was used. The solvated structure with the solvent molecules removed was used as input. The rigid framework simulation box consisted of 3 × 3 × 3 repeated unit cells. The Metropolis Monte Carlo steps were run at a fixed adsorbate pressure of 300 mbar and various temperatures. A sufficiently long run was implemented to collect statistics of loading and adsorption enthalpy.

RESULTS AND DISCUSSSION

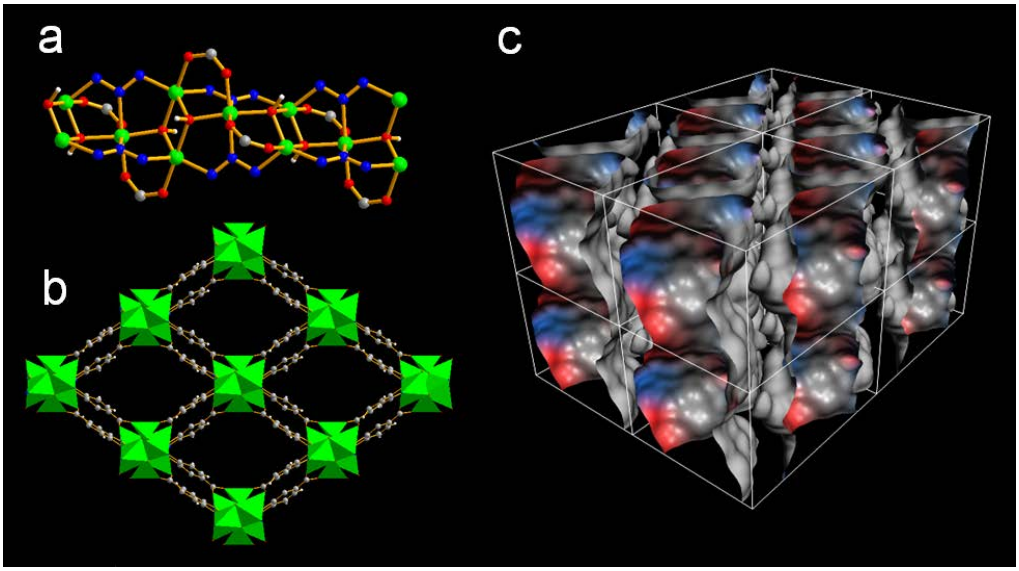

Figure 1. The rod shaped $Zn_3(OH)_2$ chains in the three-dimensional porous structure of compound **1**, for clarity only the bridging fragments of the ligands are shown (green: Zn, red: O, light gray: C, blue: N) (a); view of the structure of **1** along the *c*-axis with guests and hydrogen atoms omitted for clarity (b); Connolly surface representation of the one-dimensional channel along the *c* axis (where plain grey shows the outer surface of the pores) (c).

Brown block crystals of compound **1** were obtained by reacting zinc acetate with H_2btca in DMF/water in a Teflon-lined stainless autoclave for three days at 150 ^{o}C. The structure and composition were characterized by single crystal X-ray crystallography, powder X-ray diffraction, elemental analysis, FT-IR spectroscopy, and thermal gravimetric analysis (TGA). The crystal structure of compound **1** is analogous to that of the aluminum net in $SrAl_2$ with the "sra" topology ((see details in the Supporting Information (SI), Table S1).[50,51] In the structure of **1**, the carboxylate groups of the doubly deprotonated ligand btca act as bridges between pairs of Zn(II) ions and the triazolate moiety binds three Zn(II) ions with three different nitrogen atoms respectively resulting in alternating chains with two distorted square pyramidal metal Zn(II) centers and one octahedral metal Zn(II) center interlinked by μ_3–OH groups.[42] This structure is distinct from the MIL-53 solids, in which the exclusive octahedral units [MO_6] metal centers are connected to each other by *trans* corner sharing μ_3–OH groups to form an uniform chain. In

compound **1**, the interconnection of rod-shaped $Zn_3(OH)_2$ chains via btca linkers forms a neutral three-dimensional (3D) framework with one-dimensional (1D) nanosized rhombic channels running parallel to the crystallographic *c* axis (Figure 1). Based on the van der Waals radii of the surface atoms, the dimensions of the channels in **1** are approximately 9.5×6.7 Å. A calculation with PLATON gives a total potential solvent accessible volume of the channels of 1071.6 $Å^3$ per unit cell, or 42.1% of the total cell volume.

To quantify the amount of adsorbed solvents and the thermal stability of compound **1**, TGA was conducted in air. The TGA traces of the as-synthesized **1**·guests and the desolvated compound **1** show that the as-synthesized material contains 17.4% guests and moisture per $[Zn_3(btca)_2(OH)_2]$ formula unit and the empty structure is stable up to 350 ^oC (Figure S1, SI). FT-IR measurements indicate that the hydroxide bridging groups are retained under the desolvation conditions (Figure S2, SI). Since the powder X-ray diffraction (PXRD) pattern of compound **1** after exposure to the atmosphere (Figure S3, SI) shows sharp diffraction peaks similar to those of the as-synthesized material, the framework is largely retained during desolvation. Le Bail fitting of the powder data, reveals that the unit cell changes slightly with the cell shrinking along the *b* direction and expanding along the *a* direction reflecting the change in guests from DMF to atmospheric H_2O only, which corresponds to a 6.0% reduction in volume.

To examine the permanent porosity, methanol-exchanged compound **1** was activated at a temperature of 150 °C overnight prior to the N_2 adsorption–desorption measurement at 77 K. The N_2 adsorption–desorption measurement shows a typical type I isotherm according to the IUPAC classifications and analysis of the low pressure region (P/P_0 in the range from 0.05 to 0.25) of the N_2 adsorption branch gives an apparent Brunauer-Emmett-Teller (BET) surface area of 323 $m^2\ g^{-1}$ (Figure S4, SI). However, the CO_2 adsorption isotherms show a type I sorption

behavior with no obvious steps at 196 K. At 273K, CO_2 sorption experiments give isotherms showing hysteresis and two distinct steps, in the pressure ranges of 0–100 mbar and 400–500 mbar respectively (Figure 2), consistent with structural rearrangement to admit the guests. The first step is associated with a sharp uptake of CO_2 and a loading of three molecules per unit cell. The second step involves a more gradual uptake as the sorbent admits an additional four CO_2 molecules as the pressure reaches 1066 mbar (66.4 cm^3/g). The steps are not apparent below 1000 mbar in the CO_2 adsorption isotherms at 298K (see Figure 2a).

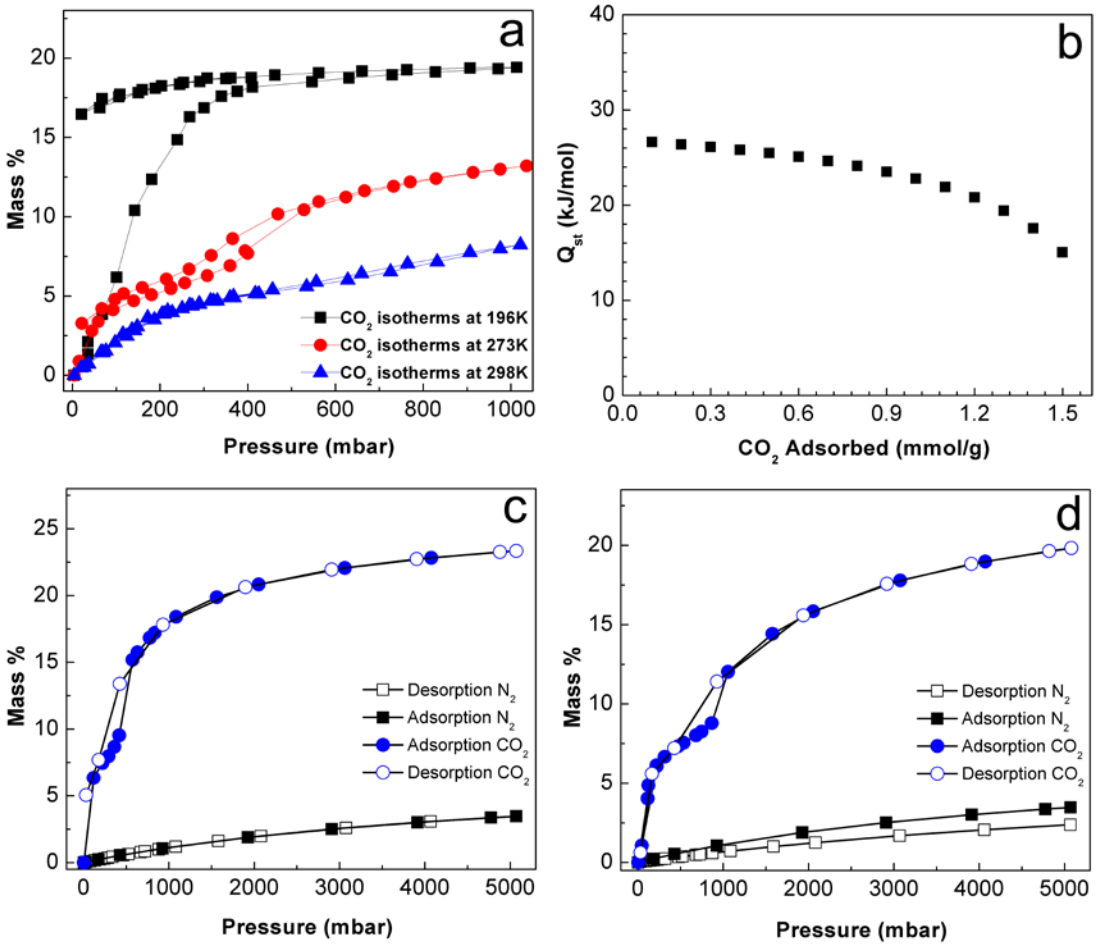

Figure 2. The CO_2 isotherms at 196, 273, 298K (a) and isosteric heat of adsorption (Q_{st}) of CO_2 calculated based on Langmuir-Freundlich equation with the adsorption data at 273 and 298K (b). High pressure isotherms of CO_2 and N_2 at 273K (c) and 298K (d), with filled/open symbols for adsorption/desorption isotherm branches.

The hysteretic behavior and appearance of two steps on the sorption branches (Figure 2a) are both significant. Pronounced sorption steps can be ascribed to transitions between relatively open and closed framework structures as gas is adsorbed with hysteresis resulting from meta-stability of the more open structure.[52] To further probe the sorption characteristics of **1**, high pressure sorption experiments with CO_2 and N_2 were conducted at two temperatures (Figures 2c, 2d). At 273 K, the step of CO_2 isotherms occurs at around 400 mbar, in accordance with the low pressure observations (Figure 2a), while a step in the CO_2 isotherms at 298 K is observed at 1000 mbar. In contrast, no steps were observed for the N_2 isotherms at 273 or 298 K over the same pressure range. These observations indicate that structural changes responsible for the steps in the isotherms not only depend on the temperature, requiring higher pressures at higher temperatures, but are also related to specific interactions of guest molecules with the framework.

To demonstrate that the framework breathing depends on the nature of the guest molecules, the variable pressure Fourier transform infrared (FT-IR) spectra of the desolvated compound **1** were recorded at different pressures of CO_2 and N_2 at 298 K (Figure 3). The band at 1560 cm^{-1}, which corresponds to a stretch asymmetric vibration, $\nu(COO^-)$,[52] of the carboxylate groups on the btca ligands, shifts as the CO_2 pressure increased to around 1400 mbar which is higher than the reshaping pressure observed from the CO_2 isotherms (Figure 2d), possibly due to the response delay to CO_2 molecules during a short equilibrium time. More notably, intensity change increases corresponding to the CO_2 pressure. However, no significant shifts in the N_2 spectra were detected for the stretching vibration of $\nu(COO^-)$. The FT-IR spectra evidently demonstrate that CO_2 molecules can induce changes in the local coordination environments around the metal centers, presumably leading to structural transition of the framework, while nitrogen does not.

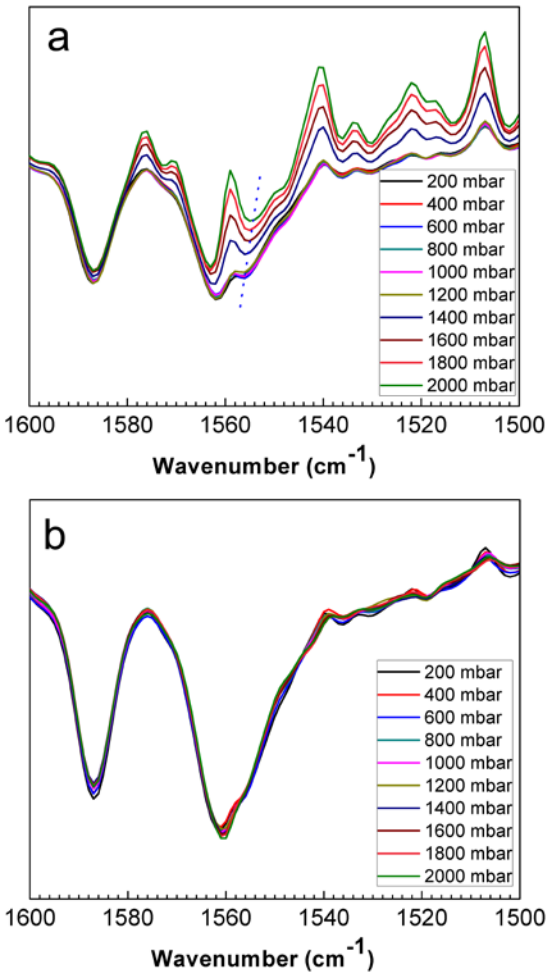

Figure 3. Variable pressure FT-IR spectra of desolvated compound **1** at various pressures under CO_2 (a) and N_2 (b) at 298K.

The desorption of CO_2 from **1** at 273K was investigated using classical molecular dynamics (MD) simulations.[53,54] Starting from a supercell loaded with the equivalent of 12 molecules of CO_2 per unit cell, a series of NσT ensemble molecular dynamics simulations were carried out. After collection of statistics for each simulation, a number of CO_2 molecules were randomly removed from the simulation cell, followed by re-equilibration and further simulations. The enthalpies of loading and cell volume from the series of simulations are shown in Figure 4(a). The results from an analogous series of simulations for MIL-53 are shown in figure 4(b) for comparison. The loading enthalpies reveal that up to a loading of about 3 molecules of CO_2 per

unit cell, the loading enthalpy is fairly constant at approximately -40 kJ mol^{-1} and the cell volume increases smoothly. Between 3 and 5 molecules of CO_2 per unit cell, the loading enthalpy increases sharply and there is a slight upward trend in the volume curve. Between loadings of 5 and 11 CO_2 molecules per unit cell, the loading enthalpy remains roughly constant with a gradual increase in cell volume (Figure 4a, inset).

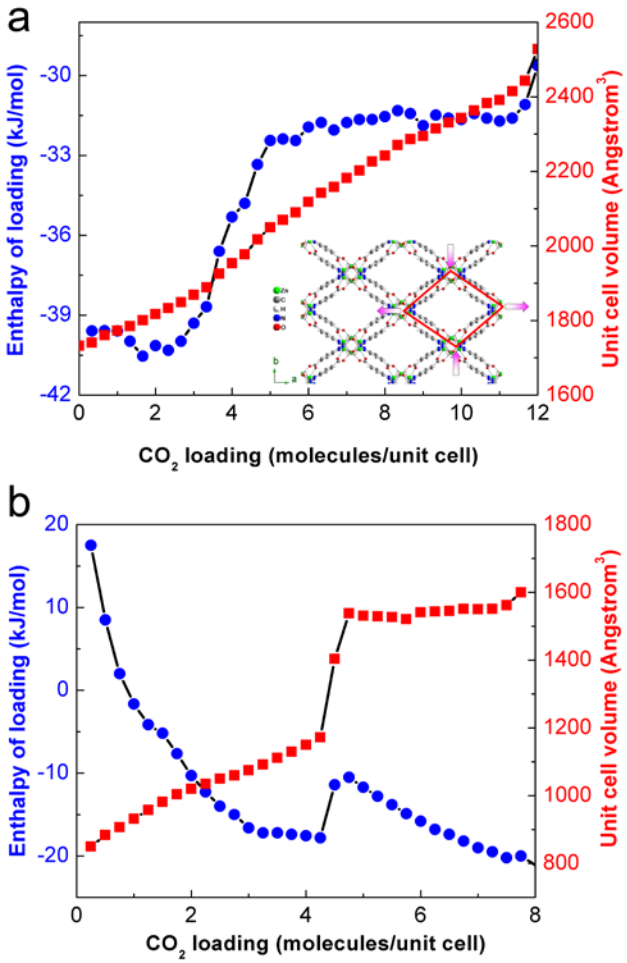

Figure 4. The loading enthalpy (blue) and cell volume (red) *vs* CO_2 loading calculated using molecular dynamics simulations at 273K (a) for compound **1** and the expansion of the channels with the increasing pressure (inset) and (b) for MIL-53.

The CO_2 sorption behavior of compound **1** contrasts with that of other reported flexible MOF materials, such as the breathing MIL-53 series and the adaptable peptide-based

$[Zn(GlyAla)_2]\cdot(guests)$.[53] It neither switches between open and closed structures like MIL-53 (Figure 4b),[10] which exhibits both an energy barrier and sudden change in cell volume, nor is there an initial barrier to sorption followed by a continuum of configurations available as it expands once the barrier is overcome, as in $Zn(GlyAla)_2$.[53] The steps in the isotherm and the simulations show that the structure opens quite easily for CO_2, reaches a plateau where sorption becomes more difficult and then opens even more at slightly higher pressures. In desolvated **1**, the structure is under strain and so the initial sorption of about 3 CO_2 molecules per unit cell is relatively easy. Once the structure has opened to its full extent, it becomes more difficult to fit more CO_2 in. The sharp increase in loading enthalpy followed by a plateau (in the absence of a transition the enthalpy would continue to increase with loading) and the second step in the isotherm show a structural transition that opens the pore volume and allows further sorption. The rigidity of the btca ligand in compound **1** combined with two different binding modes at each end is responsible for such a structural transition. The btca ligand, like the benzene-dicarboxylate, possesses few internal degrees of freedom and is less flexible than the triazolate, and hence produces a more rigid coordination to the metal. In addition to the hard and soft nature respectively of the carboxylate and azolate moieties of the btca ligand, the presence of 5-coordinate Zn ions can also play a role in the response of compound **1** to guest molecules. The presence of a free coordination around the metal could be instrumental in enabling the gradual opening of the framework, rather than the concerted opening mechanism observed in MIL-53, where the metal ions are 6-coordinate.[42] The structural transition mechanism is also different from the expansion/shrinkage upon solvent adsorption/desorption in the network of the MIL-88 family. It should be noted, however, that these transitions all depend on interactions between the guests and the skeleton.[41]

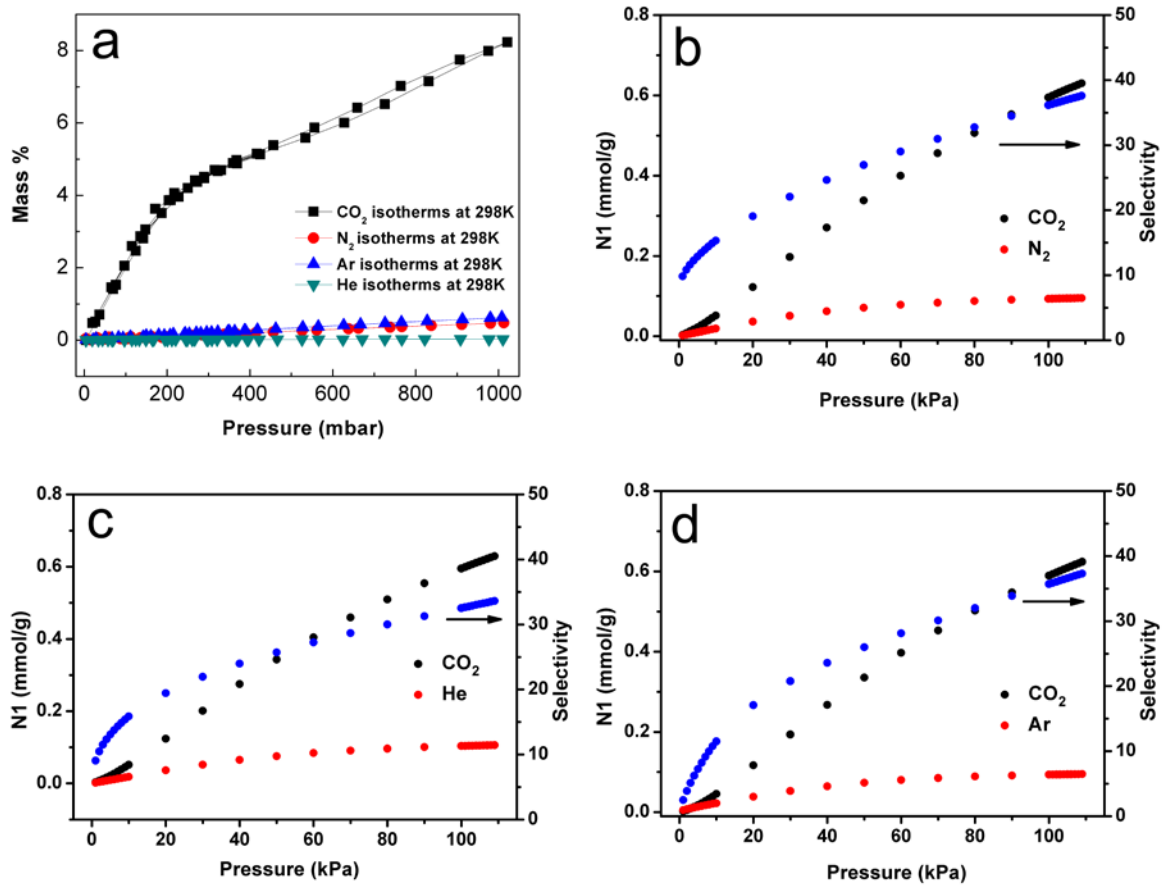

Figure 5. The CO_2, N_2, Ar, and He isotherms at 298 K (a), mixture adsorption isotherms and adsorption selectivity predicted by IAST of desolvated compound **1** at 298 K for CO_2 (15 %) and N_2 (85 %) (b), for CO_2 (15 %) and He (85 %) (c), and for CO_2 (15 %) and Ar (85 %) (d).

In order to predict CO_2/N_2, CO_2/Ar and CO_2/He binary mixture selectivity, an ideal adsorbed solution theory (IAST) calculation based on a dual-site Langmuir-Freundlich (DSLF) simulation was employed on the basis of the single-component CO_2, N_2, Ar, and He adsorption isotherms (see details in the SI, Table S2).[55,56] The sorption behavior of compound **1** makes it potentially interesting for application in gas separation. The selectivity of **1** towards CO_2/N_2, CO_2/Ar and CO_2/He was investigated at 298 K. Figure 5 shows the predicted mixture adsorption isotherms and adsorption selectivity of desolvated compound **1** for CO_2 (15 %) and N_2 (85 %), a mimic of real flue gas, with a highly selective adsorption of CO_2/N_2, CO_2/Ar, and CO_2/He of 36.3, 32.6,

and 35.9, respectively. Compound **1** preferentially adsorbs CO_2 over N_2, Ar and He, indicating that the CO_2 molecules have a relatively high affinity to inner surface of the framework and making **1** an appealing candidate to separate CO_2 from gas mixtures. One possible reason for the selective gas adsorption of compound **1** is attributable to the amplitude and kinetics of the pore opening and is a function of the interactions between the framework and the guest molecules.[57–59]

To understand the CO_2-induced structural reshaping and high selectivity to other gases, we conducted grand canonical Monte Carlo simulations (GCMC). The interaction between the framework and adsorbed molecules, quantified in terms of isosteric heats of adsorption, is presented in Table S3. The strong interaction between CO_2 and the MOF framework is evident, especially at 273 K, which probably leads to the pore opening and improved adsorption. Interactions of other adsorbate molecules are too moderate to induce conformational transition of the pores. Also note that the elevated temperature gives rise to reduced CO_2 adsorption, leading to a much weaker interaction with the MOF framework. Hence, there is no gate opening seen at 298 K below 1 bar.

CONCLUSIONS

In contrast to other reported flexible MOFs, the compound of interest belongs to a new class of flexible MOFs with unique dynamic gas adsorption behaviours demonstrated experimentally and computationally. The dynamic adsorption process is adsorbate dependent, *i.e.*, carbon dioxide molecules rather than N_2, He, and Ar enable the breathing effect to occur with corresponding appearance of more steps on the isotherms.

The dynamic adsorption behaviors of the flexible compound were detected by gas adsorptions at different temperatures and different pressure and confirmed by Fourier transform infrared. Interestingly, by taking advantage of the flexible nature inherent to the framework, this MOF material enables highly selective adsorption of CO_2/N_2, CO_2/Ar, and CO_2/He, which strongly depends on the interaction between the gas molecules and the framework with $CO_2 >> N_2$/Ar/He. Hence, by tuning the structural transformations that occur within flexible MOFs it is possible to devise materials with high adsorption selectivities for different species. Hence, this kind of MOF materials potentially has applications in gas separation, smart membranes, controlled release, molecular sensing, and nanotechnological devices.

ASSOCIATED CONTENT

Supporting Information

Single-crystal data, TGA, FT-IR results, and powder XRD patterns of as-made and desolvated material, tables. This information is available free of charge via the Internet at http://pubs.acs.org.

AUTHOR INFORMATION

Corresponding Author

mahurinsm@ornl.gov (SMM), banglin.chen@utsa.edu (BC), dais@ornl.gov (SD)

ACKNOWLEDGMENT

This work was supported by the U.S. Department of Energy, Office of Science, Basic Energy Sciences, Chemical Sciences, Geo-sciences, and Biosciences Division. This work was supported by the Welch Foundation (AX-1730) (BC).

REFERENCES

(1) D'Alessandro, D. M.; Smit, B.; Long, J. R. Carbon Dioxide Capture: Prospects for New Materials. *Angew. Chem. Int. Ed.* **2010**, *49*, 6058–6082.

(2) Yaghi, O. M.; O'Keeffe, M.; Ockwig, N. W.; Chae, H. K.; Eddaoudi, M.; Kim, J. Reticular Synthesis and the Design of New Materials. *Nature* **2003**, *423*, 705–714.

(3) Wang, Z.; Cohen, S. M. Postsynthetic Modification of Metal–Organic Frameworks. *Chem. Soc. Rev.* **2009**, *38*, 1315–1329.

(4) Liu, B.; Wong-Foy, A. G.; Matzger, A. J. Rapid and Enhanced Activation of Microporous Coordination Polymers by Flowing Supercritical CO_2. *Chem. Commun.* **2013**, 1419–1421.

(5) Li, B.; Wen, H.-M.; Zhou, W.; Chen, B. Porous Metal–Organic Frameworks for Gas Storage and Separation: What, How, and Why? *J. Phys. Chem. Lett*. **2014**, *5*, 3468–3479.

(6) Yue, Y.; Binder, A. J.; Song, R.; Cui, Y.; Chen, J.; Hensley, D. K.; Dai, S. Encapsulation of Large Dye Molecules in Hhierarchically Superstructured Metal–Organic Frameworks. *Dalton Trans*. **2014**, *43*, 17893–17898.

(7) Shimizu, G. K. H.; Vaidhyanathan, R.; Taylor, J. M. Phosphonate and Sulfonate Metal Organic Frameworks. *Chem. Soc. Rev*. **2009**, *38*, 1430–1449.

(8) Farha, O. K.; Wilmer, C. E.; Eryazici, I.; Hauser, B. G.; Parilla, P. A.; O'Neill, K.; Sarjeant, A. A.; Nguyen, S. T.; Snurr, R. Q.; Hupp, J. T. Designing Higher Surface Area Metal–Organic Frameworks: Are Triple Bonds Better Than Phenyls? *J. Am. Chem. Soc.* **2012**, *134*, 9860–9863.

(9) Moulton, B.; Zaworotko, M. J. From Molecules to Crystal Engineering: Supramolecular Isomerism and Polymorphism in Network Solids. *Chem. Rev*. **2001**, *101*, 1629–1658.

(10) Yang, S.; Lin, X.; Lewis, W.; Suyetin, M.; Bichoutskaia, E.; Parker, J. E.; Tang, C. C.; Allan, D. R.; Rizkallah, P. J.; Hubberstey, P.; et al. A Partially Interpenetrated Metal–Organic Framework for Selective Hysteretic Srption of Carbon Dioxide. *Nat. Mater*. **2012**, *11*, 710–716.

(11) Yamada, T.; Iwakiri, S.; Hara, T.; Kanaizuka, K.; Kurmoo, M.; Kitagawa, H. Porous Interpenetrating Metal-Organic Frameworks with Hierarchical Nodes. *Cryst. Growth Des*. **2011**, *11*, 1798–1806.

(12) Sato, H.; Kosaka, W.; Matsuda, R.; Hori, A.; Hijikata, Y.; Belosludov, R. V.; Sakaki, S.; Takata, M.; Kitagawa, S. Self-Accelerating CO Sorption in a Soft Nanoporous Crystal. *Science* **2014**, *343*, 167–170.

(13) Khlobystov, A. N.; Blake, A. J.; Champness, N. R.; Lemenovskii, D. A.; Majouga, A. G.; Zyk, N. V.; Schröder, M. Supramolecular Design of One-Dimensional Coordination Polymers Based on Silver(I) Complexes of Aromatic Nitrogen-Donor Ligands. *Coord. Chem. Rev*. **2001**, *222*, 155–192.

(14) Li, J. R.; Kuppler, R.-J.; Zhou, H.-C. Selective Gas Adsorption and Separation in Metal–Organic Frameworks. *Chem. Soc. Rev*. **2009**, *38*, 1477–1504.

(15) Xin, Z.; Bai, J.; Pan, Y.; Zaworotko, M. J. Synthesis and Enhanced H_2 Adsorption Properties of a Mesoporous Nanocrystal of MOF-5: Controlling Nano-/Mesostructures of MOFs To Improve Their H_2 Heat of Adsorption. *Chem. Eur. J*. **2010**, *16*, 13049–13052.

(16) Ben, T.; Lu, C. J.; Pei, C. Y.; Xu, S. X.; Qiu, S. L. Polymer-Supported and Free-Standing Metal–Organic Framework Membrane. *Chem. Eur. J*. **2012**, *18*, 10250–10253.

(17) Klein, N.; Senkovska, I.; Gedrich, K.; Stoeck, U.; Henschel, A.; Mueller, U.; Kaskel, S. A Mesoporous Metal–Organic Framework. *Angew. Chem. Int. Ed.* **2009**, *48*, 9954–9957.

(18) Cliffe, M. J.; Mottillo, C.; Stein, R. S.; Bučar, D. K.; Friščić, T. Accelerated Aging: a Low Energy, Solvent-Free Alternative to Solvothermal and Mechanochemical Synthesis of Metal–Organic Materials. *Chem. Sci.* **2012**, *3*, 2495–2500.

(19) Zheng, S. T.; Wu, T; Chou, C. T.; Fuhr, A.; Feng, P. Y.; Bu, X. H. Mimicking Zeolite to Its Core: Porous Sodalite Cages as Hangers for Pendant Trimeric $M_3(OH)$ Clusters (M = Mg, Mn, Co, Ni, Cd). *J. Am. Chem. Soc.* **2012**, *134*, 1934–1937.

(20) Liu, C.; Li, T.; Rosi, N. L. Strain-Promoted "Click" Modification of a Mesoporous Metal–Organic Framework. *J. Am. Chem. Soc.* **2012**, *134*, 18886–18888.

(21) Zhang, J. P.; Zhang, Y. B.; Lin, J. B.; Chen, X. M. Metal Azolate Frameworks: From Crystal Engineering to Functional Materials. *Chem. Rev.* **2012**, *112*, 1001–1033.

(22) Ma, L.; Abney, C.; Lin, W. Enantioselective Catalysis with Homochiral Metal–Organic Frameworks. *Chem. Soc. Rev.* **2009**, *38*, 1248–1256.

(23) Cui, Y.; Yue, Y.; Qian, G.; Chen, B. Luminescent Functional Metal–Organic Frameworks. *Chem. Rev.* **2012**, *112*, 1126–1162.

(24) Sun, L.-B.; Li, J.-R.; Park, J.; Zhou, H.-C. Cooperative Template-Directed Assembly of Mesoporous Metal–Organic Frameworks. *J. Am. Chem. Soc.* **2012**, *134*, 126–129.

(25) Lykourinou, V.; Chen, Y.; Wang, X.-S.; Meng, L.; Hoang, T.; Ming, L.-J.; Musselman, R. L.; Ma, S. Immobilization of MP-11 into a Mesoporous Metal–Organic Framework, MP-11@mesoMOF: A New Platform for Enzymatic Catalysis. *J. Am. Chem. Soc.* **2011**, *133*, 10382–10385.

(26) Greenaway, A.; Gonzalez-Santiago, B.; Donaldson, P. M.; Frogley, M. D.; Cinque, G.; Sotelo, J.; Moggach, S.; Shiko, E.; Brandani, S.; Howe, R. F.; et al. In situ Synchrotron IR Microspectroscopy of CO_2 Adsorption on Single Crystals of the Functionalized MOF Sc_2(BDC-$NH_2)_3$. *Angew. Chem. Int. Ed.* **2014**, *53*, 13483–13487.

(27) Erucar, I.; Keskin, S. Separation of CO_2 Mixtures Using Zn(bdc)$(ted)_{0.5}$ Membranes and Composites: A Molecular Simulation Study. *J. Phys. Chem. C* **2011**, *115*, 13637–13644.

(28) Fateeva, A.; Chater, P. A.; Ireland, C. P.; Tahir, A. A.; Khimyak, Y. Z.; Wiper, P. V.; Darwent, J. R.; Rosseinsky, M. J. A Water-Stable Porphyrin-Based Metal–Organic Framework Active for Visible-Light Photocatalysis. *Angew. Chem. Int. Ed*. **2012**, *51*, 7440–7444.

(29) Gassensmith, J. J.; Kim, J. Y.; Holcroft, J. M.; Farha, O. K.; Stoddart, J. F.; Hupp, J. T.; Jeong, N. C. A Metal–Organic Framework–Based Material for Electrochemical Sensing of Carbon Dioxide. *J. Am. Chem. Soc*. **2014**, *136*, 8277–8282.

(30) Yue, Y.; Qiao, Z.–A.; Fulvio, P. F.; Binder, A. J.; Tian, C.; Chen, J.; Nelson, K. M.; Zhu, X.; Dai, S. Template-Free Synthesis of Hierarchical Porous Metal–Organic Frameworks. *J. Am. Chem. Soc*. **2013**, *135*, 9572–9575.

(31) Liu, Y.; Her, J.-H.; Dailly, A.; Ramirez-Cuesta, A. J.; Neumann, D. A.; Brown, C. M. Reversible Structural Transition in MIL-53 with Large Temperature Hysteresis. *J. Am. Chem. Soc.* **2008**, *130*, 11813–11818.

(32) Kolokolov, D. I.; Jobic, H.; Stepanov, A. G.; Guillerm, V.; Devic, T.; Serre, C.; Férey G. Dynamics of Benzene Rings in MIL-53(Cr) and MIL-47(V) Frameworks Studied by ^{2}H NMR Spectroscopy. *Angew. Chem. Int. Ed*. **2010**, *49*, 4791–4794.

(33) Llewellyn, P. L.; Maurin, G.; Devic, T.; Loera-Serna, S.; Rosenbach, N.; Serre, C.; Bourrelly, S.; Horcajada, P.; Filinchuk, Y.; Férey, G. Prediction of the Conditions for Breathing

of Metal Organic Framework Materials Using a Combination of X-ray Powder Diffraction, Microcalorimetry, and Molecular Simulation. *J. Am. Chem. Soc.* **2008**, *130*, 12808–12814.

(34) Kitagawa, S.; Uemura, K. Dynamic Porous Properties of Coordination Polymers Inspired by Hydrogen Bonds. *Chem. Soc. Rev*. **2005**, *34*, 109–119.

(35) Chen, B.; Ma, S.; Hurtado, E. J.; Lobkovsky, E. B.; Liang, C.; Zhu, H.; Dai, S. Selective Gas Sorption within a Dynamic Metal-Organic Framework. *Inorg. Chem*. **2007**, *46*, 8705–8709.

(36) Horike, S.; Shimomura, S.; Kitagawa, S. Soft Porous Crystals. *Nat. Chem.* **2009**, *1*, 695–704.

(37) Gücüyener, C.; van den Bergh, J.; Gascon, J.; Kapteijn, F. Ethane/Ethene Separation Turned on Its Head: Selective Ethane Adsorption on the Metal−Organic Framework ZIF-7 through a Gate-Opening Mechanism. *J. Am. Chem. Soc.* **2010**, *132*, 17704–17706.

(38) Serre, C.; Bourrelly, S.; Vimont, A.; Ramsahye, N. A.; Maurin, G.; Llewellyn, P. L.; Daturi, M.; Filinchuk, Y.; Leynaud, O.; Barnes, P.; et al. An Explanation for the Very Large Breathing Effect of a Metal–Organic Framework during CO_2 Adsorption. *Adv. Mater*. **2007**, *19*, 2246–2251.

(39) Martí-Gastaldo, C.; Antypov, D.; Warren, J. E.; Briggs, M. E.; Chater, P. A.; Wiper, P. V.; Miller, G. J.; Khimyak, Y. Z.; Darling, G. R.; Berry, N. G.; et al. Side-Chain Control of Porosity Closure in Single- and Multiple-Peptide-Based Porous Materials by Cooperative Folding. *Nat. Chem.* **2014**, *6*, 343–351.

(40) Férey, G.; Serre, C.; Devic, T.; Maurin, G.; Jobic, H.; Llewellyn, P. L.; De Weireld, G.; Vimont, A.; Daturif M.; Chang, J.-S. Why Hybrid Porous Solids Capture Greenhouse Gases? *Chem. Soc. Rev*. **2011**, *40*, 550–562.

(41) Serre, C.; Mellot-Draznieks, C.;Surblé, S.; Audebrand, N.; Filinchuk, Y.; Férey, G. Role of Solvent-Host Interactions That Lead to Very Large Swelling of Hybrid Frameworks. *Science* **2007**, *315*, 1828–1831.

(42) Bourrelly, S.; Llewellyn, P. L.; Serre, C.; Millange, F.; Loiseau, T.; Férey G. Different Adsorption Behaviors of Methane and Carbon Dioxide in the Isotypic Nanoporous Metal Terephthalates MIL-53 and MIL-47. *J. Am. Chem. Soc.* **2005**, *127*, 13519–13521.

(43) Thallapally, P. K.; Tian, J.; Kishan, M. R.; Fernandez, C. A.; Dalgarno, S. J.; McGrail, P. B.; Warren, G. E.; Atwood, J. L. Flexible (Breathing) Interpenetrated Metal−Organic Frameworks for CO_2 Separation Applications. *J. Am. Chem. Soc*. **2008**, *130*, 16842–16843.

(44) Loiseau, T.; Serre, C.; Huguenard, C.; Fink, G.; Taulelle, F.; Henry, M.; Bataille, T.; Férey, G. A Rationale for the Large Breathing of the Porous Aluminum Terephthalate (MIL-53) Upon Hydration. *Chem. Eur. J.* **2004**, *10*, 1373–1382.

(45) Barthelet, K.; Marrot, J.; Riou, D.; Férey, G. A Breathing Hybrid Organic–Inorganic Solid with Very Large Pores and High Magnetic Characteristics. *Angew. Chem., Int. Ed*. **2002**, *41*, 281–284.

(46) Platero-Prats, A. E.; de la Peña-O'Shea, V. A.; Snejko, N.; Monge, Á.; Gutiérrez-Puebla, E. Dynamic Calcium Metal–Organic Framework Acts as a Selective Organic Solvent Sponge. *Chem. Eur. J.* **2010**, *16*, 11632–11640.

(47) Toby, B. EXPGUI, A Graphical User Interface for GSAS. *J. Appl. Crystallogr*. **2001**, *34*, 210–213.

(48) Sheldrick, G. M. SADABS, Program for Empirical Absorption Correction of Area Detector Data; University of Göttingen, Germany, **1996**.

(49) Sheldrick, G. M. SHELXL-97, University of Göttingen, Göttingen, Germany, **1997**.

(50) Zhang, X.-M.; Hao, Z.-M.; Zhang, W.-X.; Chen, X.-M. Dehydration-Induced Conversion from a Single-Chain Magnet into a Metamagnet in a Homometallic Nanoporous Metal–Organic Framework. *Angew. Chem. Int. Ed*. **2007**, *46*, 3456–3459.

(51) Rosi, N. L.; Kim, J.; Eddaoudi, M.; Chen, B.; O'Keeffe, M.; Yaghi, O. M. Rod Packings and Metal−Organic Frameworks Constructed from Rod-Shaped Secondary Building Units. *J. Am. Chem. Soc*. **2005**, *127*, 1504–1518.

(52) Zhang, Y.; Bo, X.; Luhana, C.; Wang, H.; Li, M.; Guo, L. Facile Synthesis of a Cu-based MOF Confined in Macroporous Carbon Hybrid Material with Enhanced Electrocatalytic Ability. *Chem. Commun*. **2013**, *49*, 6885–6887.

(53) Rabone, J.; Yue, Y.-F.; Chong, S. Y.; Stylianou, K. C.; Bacsa, J.; Bradshaw, D.; Darling, G. R.; Berry, N. G.; Khimyak, Y. Z.; Ganin, A. Y.; et al. An Adaptable Peptide-Based Porous Material. *Science* **2010**, *329*, 1053–1057.

(54) Chen, L.; Mowat, J. P. S.; Fairen-Jimenez, D.; Morrison C. A.; Thompson, S. P.; Wright P. A.; Düren, T. Elucidating the Breathing of the Metal–Organic Framework MIL-53(Sc) with ab Initio Molecular Dynamics Simulations and in Situ X-ray Powder Diffraction Experiments. *J. Am. Chem. Soc.* **2013**, *135*, 15763–15773.

(55) Cessford, N. F.; Seaton, N. A.; Düren T. Evaluation of Ideal Adsorbed Solution Theory as a Tool for the Design of Metal-Organic Framework Materials. *Ind. Eng. Chem. Res*. **2012**, *51*, 4911–4921.

(56) Bae, Y.-S.; Mulfort, K. L.; Frost, H.; Ryan, P.; Punnathanam, S.; Broadbelt, L. J.; Hupp, J. T.; Snurr, R. Q. Separation of CO_2 from CH_4 Using Mixed-Ligand Metal−Organic Frameworks. *Langmuir* **2008**, *24*, 8592–8598.

(57) Choi, H.-S.; Suh, M. P. Highly Selective CO_2 Capture in Flexible 3D Coordination Polymer Networks. *Angew. Chem. Int. Ed*. **2009**, *48*, 6865–6869.

(58) Chen, B.; Xiang, S.; Qian, G. Metal−Organic Frameworks with Functional Pores for Recognition of Small Molecules. *Acc. Chem. Res.* **2010**, *43*, 1115–1124.

(59) Chen, B.; Liang, C.; Yang, J.; Contreras, D. S.; Clancy, Y. L.; Lobkovsky, E. B.; Yaghi, O. M.; Dai, S. A Microporous Metal–Organic Framework for Gas-Chromatographic Separation of Alkanes. *Angew. Chem. Int. Ed*. **2006**, *45*, 1390–1393.

TOC

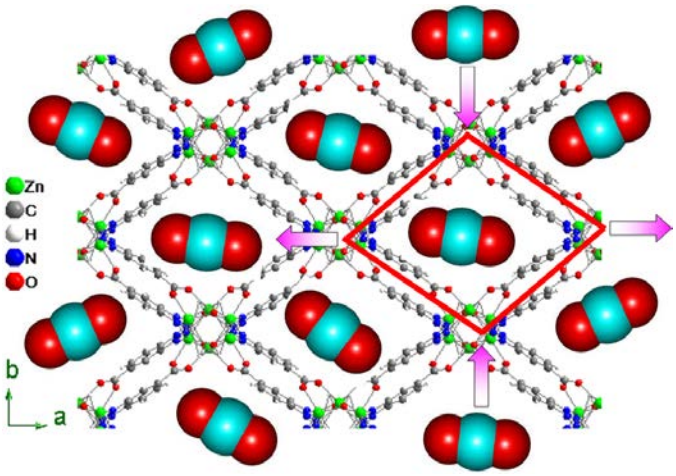

A flexible metal-organic framework that exhibited guest molecule-controlled dynamic gas adsorption in which carbon dioxide molecules rather than N_2, He, and Ar induce a structural transition with a corresponding appearance of additional steps in the isotherms was detected by gas adsorptions at different temperatures and different pressures and confirmed by variable pressure Fourier transform infrared and molecular simulations.